*DOI:*
10.1109/TBME.2016.2574619

*Document Version*
Peer reviewed version

# Personalized Models of Human Atrial Electrophysiology Derived From Endocardial Electrograms

C. Corrado*, J. Whitaker, H. Chubb, S. Williams, M. Wright, J. Gill, M. O'Neill and S.A. Niederer

***Abstract*—Objective: Computational models represent a novel framework for understanding the mechanisms behind atrial fibrillation (AF) and offer a pathway for personalizing and optimizing treatment. The characterization of local electrophysiological properties across the atria during procedures remains a challenge. The aim of this work is to characterize the regional properties of the human atrium from multi-electrode catheter measurements. Methods: We propose a novel method that characterizes regional electrophysiology properties by fitting parameters of an ionic model to conduction velocity and effective refractory period restitution curves obtained by a $s_1\_s_2$ pacing protocol applied through a multi-electrode catheter. Using an in-silico data set we demonstrate that the fitting method can constrain parameters with a mean error of $21.9 \pm 16.1\%$ and can replicate conduction velocity and effective refractory curves not used in the original fitting with a relative error of $4.4 \pm 6.9\%$. Results: We demonstrate this parameter estimation approach on 5 clinical data sets recorded from AF patients. Recordings and parametrization took approx 5 and 6 minutes, respectively. Models fitted restitution curves with an error of $\sim 5\%$ and identify a unique parameter set. Tissue properties were predicted using a 2D atrial tissue sheet model. Spiral wave stability in each case was predicted using tissue simulations, identifying distinct stable (2/5), meandering and breaking up (2/5) and unstable self terminating (1/5) spiral tip patterns for different cases. Conclusion and significance: We have developed and demonstrated a robust and rapid approach for personalizing local ionic models from a clinically tractable protocol to characterize cellular properties and predict tissue electrophysiological function.**

***Index Terms*—Electrograms, atrial fibrillation, catheter measurements, computational models, model personalization, restitution curves, conduction velocity, effective refractory period**

## I. Introduction

Atrial fibrillation (AF) is a supra-ventricular tachyarrhythmia characterized by uncoordinated atrial activation with consequent deterioration of mechanical function. AF is the most common arrhythmia, affecting almost 2.5 million people in the US, [1] and is associated with an increased incidence of cardiovascular disease, stroke and premature death.

AF is commonly treated by radio frequency catheter ablation in drug refractory patients, [2], [3], [4]. However, many patients require multiple procedures to achieve sinus rhythm [5]. No consensus regarding the mechanisms that sustain fibrillation in the atrium has been reached; however local tissue properties, identified by complex fractionated electrograms [6] and focal impulse and rotor activation patterns [7], [8], and a heterogeneous atrial substrate [9] have been proposed to play a role in the induction and maintenance of AF.

Biophysical modeling provides a formal framework that combines our understanding of atrial physiology, physical constraints and patient measurements to make quantitative predictions of patient response to treatment. The models characterize the local cellular ionic properties, conductivity and propagation of electrical activation across myocardial tissue. These models have provided insights into the fundamental mechanisms responsible for arrhythmias in the ventricles and atria, [10], and have the capacity to optimize treatment plans for an individual patient's pathology. However, current models have failed to capture individual variation in electrophysiological properties across the atria that are potentially crucial to representing the individual's pathology.

Characterizing the parameters of cellular ionic model across patient's atria is crucial for simulating the effects of tissue heterogeneity on AF. In this study we develop a clinically tractable protocol to quantify local tissue properties and encode them within a model of cellular electrophysiology. The study is separated into three sections. Firstly, we have quantified the accuracy of the model fitting protocol using in-silico data sets. Secondly, the fitting approach is applied to clinical measurements recorded from five cases. Finally, the potential clinical utility of this approach is demonstrated by using the fitted models to predict if characterized tissue regions can sustain a re-entrant spiral activation patterns and are potential ablation targets.

## II. Methods

### A. Computational model

In this section we introduce the computational model adopted for simulating the propagation of the electrical stimulus across the atrial tissue. This model aims to numerically



Manuscript received ...; revised ...; accepted ...

This work was supported by the British Heart Foundation (PG\13\37\30280) and the Department of Health via the National Institute for Health Research (NIHR) comprehensive Biomedical Research Centre award to Guy's & St Thomas' NHS Foundation Trust in partnership with King's College London and King's College Hospital NHS Foundation Trust.

C. Corrado* J. Whitaker, H. Chubb, S. Williams, M. Wright, J. Gill, M. O'Neill and S.A. Niederer are with the Biomedical Engineering Department, King's College London, London SE17EH, UK.

* corresponding author: cesare.corrado@kcl.ac.uk

This paper has supplementary downloadable material available at http://ieeexplore.ieee.org, provided by the authors. This includes five multimedia mpg format movie clips, which shows tissue simulations for the 5 identified parameter sets. This material is 96 Mb in size.

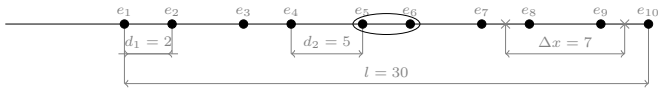


Figure 1. Decapolar catheter configuration and dimensions. Dimensions are expressed in $\mathrm{mm}$ Bipolar electrodes are determined by pairs ($e_1$,$e_2$),($e_3$,$e_4$), ($e_5$,$e_6$), ($e_7$,$e_8$) and ($e_9$,$e_{10}$). The pacing stimulus is applied to the central poles, ($e_5$,$e_6$), highlighted by the gray ellipse

simulate catheter recordings to reproduce clinical electrograms.

Atrial tissue electrophysiology was modeled by the monodomain simplification, [11], of the bi-domain electrophysiology model, [12], when intra- and extra- cellular conductivities are considered proportional up to a constant $\lambda$. To simulate recordings from a decapolar catheter a model of a 1D strip of atrial tissue was created. The decapolar catheter electrodes were placed along the tissue strip as shown in Fig. 1. The model was stimulated from electrodes ($e_5$,$e_6$) and bipolar recordings were calculated from the difference in extracellular potentials at electrode pairs ($e_1$,$e_2$), ($e_3$,$e_4$), ($e_7$,$e_8$) and ($e_9$,$e_{10}$). The distance ($\Delta x$) between pairs of electrodes for calculating conduction velocity corresponds to the distance between the baricentres of electrode pairs. Dimensions of the decapolar catheter are reported in Fig. 1.

The monodomain equations were discretized in space with a first order Finite Element Method (FEM) on a domain of length $L = 20\,\mathrm{cm}$ and with a discretization step of $dx = 200\,\mu\mathrm{m}$. Time discretization of the partial differential equations were performed with the semi-implicit backward Euler method presented in [13], with a fixed time step of $dt = 0.1\,\mathrm{ms}$. No mass lumping was applied. Electrograms were sampled at a rate of $5\,\mathrm{kHz}$. Simulations were performed on the UK national super computing facility ARCHER.

### B. Choice of the ionic model

The ionic model was chosen to have the smallest number of parameters while capturing the measured CV and ERP restitution properties. Model complexity was selected to reflect the available clinical data. Physiological mechanisms, including cardiac memory and intracellular calcium handling were not recorded and so were not included in the model.

As clinical data were recorded using conventional catheters, only local activation time measurements are available; repolarisation times can not be reliably recorded from conventional catheters on human atria. Thus, an $s_1\_s_2$ protocol, as described in section II-C, will not provide a dynamic restitution curve for each $s_1$, but it provides only an estimate of the steady state ERP for the $s_1$ values evaluated. To estimate a dynamic ERP restitution curve would require the addition of a third stimulus that would need to be decremented, to estimate the ERP of each $s_2$ pacing interval. This would drastically increase the duration of the protocol reducing our ability to use this approach to map multiple sites in the clinical setting. We thus adopt an ionic model that can be characterized by the available clinical measurements.

Two of the simplest models of cardiac physiology, that have a sharp upstroke, are the Aliev Panfilov (AP), [14] and

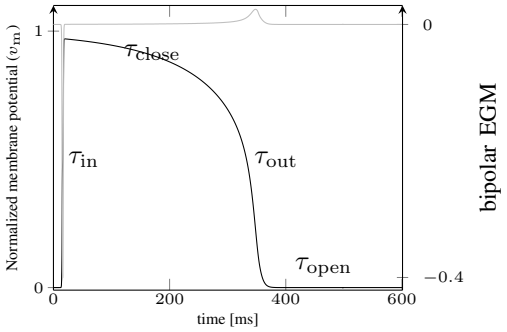


Figure 2. Example of trans-membrane potential (——) and bipolar electrode output (——). Trans-membrane potential was evaluated as the mean of the trans-membrane potentials of the two poles constituting the electrode

Mitchell Schaeffer (MS), [15]. Each model has four ionic parameters and one diffusion coefficient parameter. The MS model was chosen as it is formulated in terms of depolarizing and repolarizing currents; however, the method developed here could equally be applied to the AP model. A complete description of the MS model and 1D fiber model are provided in the supplement. Fig. 2 shows a schematic of the simulated trans-membrane potential and the corresponding electrode signal. In the same Figure the parameter affecting each specific phase of the action potential (AP) is also shown.

### C. Pacing protocol and activation measurements

In clinical cases the atria were paced from the central poles ($e_5$,$e_6$) of the decapolar catheter placed on the roof of the left atrium (LA). Activation was measured from distal, ($e_1$,$e_2$), ($e_9$,$e_{10}$), and proximal, ($e_3$,$e_4$), ($e_7$,$e_8$), poles in a bipolar configuration, with sampling frequency of $1\,\mathrm{kHz}$ (data set 1) and $4\,\mathrm{kHz}$ (data sets 2,3,4,5). A Biotronik UHS 300 device stimulator was used. A $s_1\_s_2$ protocol was applied with $s_1 = 300$, $500$ and $600\,\mathrm{ms}$, (data set 1-4) and $s_1 = 300$, $500$ and $700\,\mathrm{ms}$ (data set 5) and $s_2$ values starting at $280$, $400$ and $500\,\mathrm{ms}$, respectively. For each $s_1$ pacing rate, $s_2$ was decremented by $20\mathrm{ms}$, down to the first $s_2$ that did not capture, identifying the ERP.

Before each premature $s_2$ stimulus was applied, the tissue was pre-paced with 8 stimuli with a temporal interval of $s_1$ to confirm reliable capture and achieve a steady state of activity. The chosen pacing protocol required $< 5\,\mathrm{min}$ for its application.

For each bi-polar electrogram lead and for each inter-pacing interval the non-linear energy operator (NLEO), [16], was evaluated and filtered by a zero-phase window-based finite impulse response digital filter, [17] to eliminate oscillations. The time the electrical stimulus is applied and the stimulus duration are defined as $t^{\mathrm{stim}}$ and $\Delta t^{\mathrm{stim}}$, respectively. The activation time is defined as the time corresponding to the peak of the NLEO operator inside the time window $[(t^{\mathrm{stim}} + \Delta t^{\mathrm{stim}}),\ (t^{\mathrm{stim}} + \Delta t^{\mathrm{stim}} + \Delta t^{\mathrm{act}})]$; peaks occurring outside the time window are considered anomaly and discarded. The choice of the interval $\Delta t^{\mathrm{act}}$ was based on manual calibration to minimize identification of early or delayed artifacts as the activation time, this yielded a minimum admissible CV of

$14\,\mathrm{cm/s}$. In this work $\Delta t^{\mathrm{stim}} = 0.6\,\mathrm{ms}$, while $\Delta t^{\mathrm{act}} = 50\,\mathrm{ms}$. A manual user check and validation on the activations was performed case by case.

By stimulating from the central poles of the decapolar catheter it is possible to record two sets of activation times at the same distance from the stimulus application site. This would provide two parameter sets at each catheter location. However, due to the curvature of the atria it is not possible to guarantee good contact between all electrodes and the atrial wall at each location. In none of the cases recorded here did we collect complete proximal and distal data sets. For this reason only one model is fitted to each catheter location.

### *D. Restitutions evaluation*

In contrast to ventricular electrograms, [18], atria electrograms only display depolarization and do not show repolarization. Thus, from atrial electrograms it is possible to determine the activation time (depolarization) only. From activation times two restitution curves are directly available:

- The CV restitution. For two adjacent electrode pairs, CV is evaluated as the ratio between the inter-electrode distance, ($\Delta x$) and the time elapsed between the activation wave, generated by the premature pacing ($s_2$), propagating between the electrodes.
- The ERP restitution. For each $s_1$ inter-pacing interval, ERP represents the smallest $s_2$ premature inter-pacing stimulus where no CV is produced.

ERP accuracy depends on the decrement step adopted for $s_2$ ($20\,\mathrm{ms}$ in this work); this accuracy allows us to constrain the model parameters while still ensuring a clinically compatible protocol duration.

### *E. Parameter fitting*

Model parameters were determined by comparing the clinically recorded or simulated CV and ERP restitution data with a data base of pre-computed numerical simulations to identify the best fitting parameter set. A data base of candidate simulation results for $99840$ combinations of the model parameters summarized in Table I was created for the described pacing protocol.

Clinical data used in this article always displayed $1:1$ capture and had an ERP $\geq 200\,\mathrm{ms}$. The MS model has been reported to exhibit pacemaker behavior [19] where at the cellular scale, the MS model can spontaneously depolarize in the absence of a stimulus current, for some combinations of parameters. In the case of a tissue model, this appears as a focal activation, where a region of tissue spontaneously activates in the absence of a stimulus current or activation from a neighbouring cell. No evidence of this was found in the clinical data.

As a consequence, parameter sets with ERP $< 200\,\mathrm{ms}$, that failed to yield $1:1$ capture were excluded from the data set. To remove all parameter sets that exhibited pacemaker behavior we applied three tests to each candidate parameter set. First the model was rapidly paced ($3.33\,\mathrm{Hz}$ pacing) in a 0D model. Second, the parameter fitting pacing protocol was applied in a 1D model. Thirdly, a spiral wave was initiated in a 2D simulation (criterion for pacemaker activity are described in supplementary material). Tests one and two were evaluated on all candidate parameters, giving a final data set of $51306$ parameters sets. The third test is only performed on the fitted parameter sets to maintain computational tractability.

| | diffusion coefficient $(\mathrm{cm^2/s})$ | $\tau_{\mathrm{in}}$ (ms) | $\tau_{\mathrm{out}}$ (ms) | $\tau_{\mathrm{open}}$ (ms) | $\tau_{\mathrm{close}}$ (ms) |
|---|---|---|---|---|---|
| min | 0.25 | 0.05 | 0.5 | 65 | 65 |
| max | 4.0 | 0.4 | 9.5 | 215 | 185 |
| step | 0.75 | 0.05 | 1 | 10 | 10 |

Table I
PARAMETER VALUES USED FOR BUILDING THE DATA SET. A SET OF PARAMETER VALUES RANGING FROM THE MINIMUM TO THE MAXIMUM VALUE IN INCREMENTS OF THE STEP VALUE IS CREATED. THE DATA SET OF CANDIDATE SOLUTIONS WAS GENERATED BY MODELS WITH EACH OF THE PERMUTATIONS OF THE CARTESIAN PRODUCTS OF ALL OF THE PARAMETER VALUE SETS.

The parameter set that best fits clinical or simulated measurements is determined by the following two step algorithm:

- The candidate ERP restitution curve and maximum CV value are compared against the corresponding curves for all the $51306$ candidate parameter sets. A sub set of candidate parameter sets ($I_1$) is identified that matches the measured ERP restitution curve and have a maximum CV within $20\%$ of the recorded value.
- The $L_2$ norms of the difference between the measured CV restitution curves and the CV restitution curves for all candidate parameter sets in set $I_1$ are calculated and used to rank all candidate parameter sets.

Parameter sets that yield pacemaker behavior in 2D simulations were identified and excluded as a final check in the parameter fitting algorithm, described above, to maintain computational tractability. This approach provided a robust and rapid fitting method taking approximately $6$ minutes to find the optimal parameter set and ensure no pacemaker activity. The collective fitting performed here yields well constrained predictions, [20], [21], [22], even when individual parameters are poorly constrained.

## III. RESULTS

### *A. Validation with synthetic data*

Error properties and robustness of our approach are evaluated by first generating a set of 247 models by randomly choosing parameter values within the $[\min, \max]$ intervals reported in Table I. The test parameter set was created by generating a set of $1000$ random parameter sets and then considering only combinations that provide a $1:1$ capturing, an ERP $\geq 200\,\mathrm{ms}$, at least one non zero CV value for $s_1 = 300$ and $s_2 = 280$, and did not exhibit pacemaker behavior in 0,1 or 2D simulations. The pacing protocol was then applied with $s_1 = 300, 500$ and $600\,\mathrm{ms}$ and bipolar electrograms were numerically computed. A white noise with an intensity equal to $10\%$ of the maximum absolute value of the electrode output was added to each electrode output; restitutions were then evaluated by applying the procedure described in section II-D.

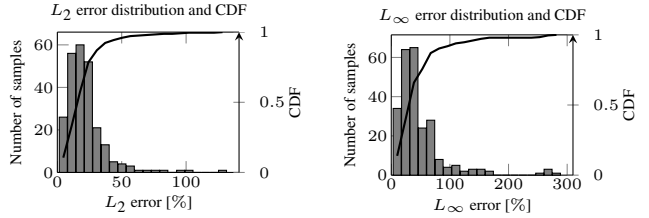


Figure 3. Left: $L_2$ error distribution (bars) and cumulative distribution (thick line) evaluated for 247 set of randomly chosen parameters. Right: $L_\infty$ error distribution (bars) and cumulative distribution (thick line) evaluated for 247 set of randomly chosen parameters.

For each of the 247 models, the parameter set determined from the fitting process was compared with the known true solution. All errors presented here are relative, reported as the percentage change between the known and the fitted value. The $L_2$ is the mean squared relative error on the 5 fitted parameters and furnishes a collective error estimate, where the contribution of each of the 5 parameters is taken into account. The $L_\infty$ is the maximum relative error across the 5 fitted parameters and furnishes an error estimate based on the the parameter affected by the maximum error only.

Fig. 3 shows the $L_2$ and $L_\infty$ error distributions and the corresponding cumulative distribution function (CDF). For the $L_2$ error, a mean error of $21.9\%$ was found with a standard deviation of $16.1\%$. As depicted by the CDF, $95\%$ of the estimated parameters analyzed here have a $L_2$ error not greater than $40\%$. For the $L_\infty$ error, a mean error of $48.1\%$ was found and a standard deviation of $43.8\%$.

In Fig. 4 the signed relative error distribution is shown for each parameter, together with the relative difference between the selected parameter set and the optimal possible parameter set based on the nearest data base parameter set to the correct values. In the same Figure (bottom, right), the number of occurrences each parameter defines the $L_\infty$ error is also reported. The best performances are obtained in estimating the diffusion coefficient ($2.5 \pm 30.6\%$), $\tau_{\text{in}}$ ($3.6 \pm 25.2\%$), $\tau_{\text{close}}$ ($1.9 \pm 26.4\%$) and $\tau_{\text{open}}$ ($2.2 \pm 22.1\%$) parameters. The parameter $\tau_{\text{out}}$ ($13.4 \pm 56.9\%$) is characterized by repolarization (Fig. 2) and is not well constrained by activation data.

To test the impact of poorly constrained parameters on simulation results we compared the predicted CV and ERP restitution curves from the estimated parameter sets and the corresponding curves from the known parameter sets with an $s_1$ pacing value of $400$ and $700$ ms that were not used in the original parameter fitting data. The $L_2$ relative errors with respect to ERP and CV restitution are evaluated for each of the 247 fitted parameter sets. Fig. 5 shows the distribution of error together with the CDF. The $L_2$ relative error was characterized by a mean value of $4.4\%$ and a standard deviation of $6.9\%$. This confirms that, even though some parameters are not tightly constrained, the fitted parameter set gives a model that functionally represents the simulations generated with the known model parameters and is compatible with predicting functional tissue properties not used in the original fitting.

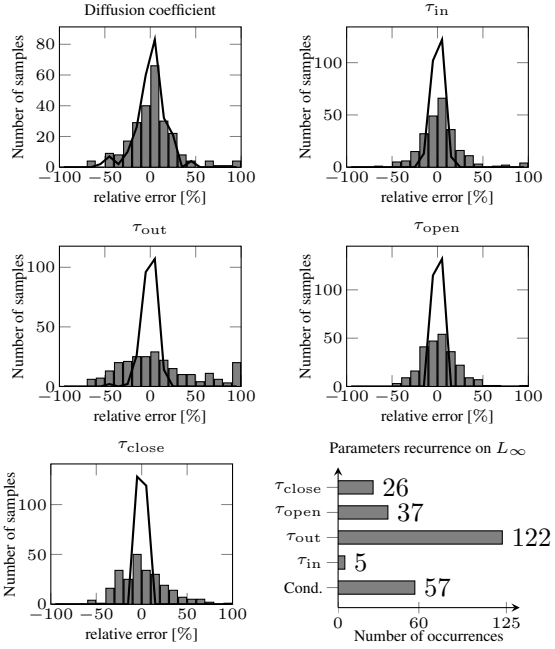


Figure 4. Error distribution bars and best error distribution obtained by choosing the nearest candidate parameter set for each of target parameter set. (lines) for each parameter. Bottom right: recurrence of the maximum error for each parameter

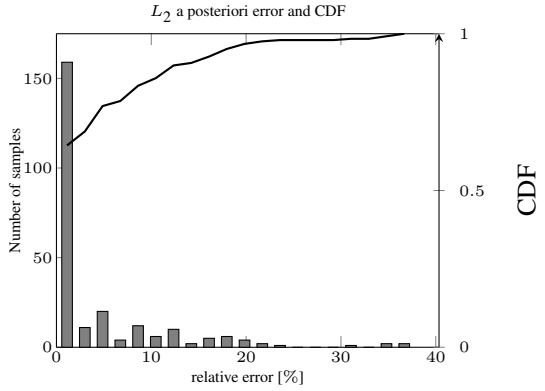


Figure 5. Error distribution and CDF for the $L_2$ error evaluated a posteriori on ERP and CV restitutions for $s_1 = [700, 400]$ ms

### *B. Application to clinical data*

The model personalization protocol was then applied to 5 data sets recorded from patients suffering paroxysmal AF. All measurements used to constrain these models are provided in the supplementary material. ERP restitution (Fig. 6, panel 4) together with the maximum CV values were used to reduce the number of candidate parameter sets; CV restitutions (Fig. 6, panels 1-3) were then fitted to 30 measurements with different $s_1\_s_2$ combinations the 3 curves generated for each $s_1$ pacing rate. A unique parameter set was identified for each patient in 1 minute. Testing for 2D pacemaker behavior took a further 5 minutes. Estimated model parameters for each data set are summarized in Table II. Fitted ERP and CV restitution curves are shown in Fig. 6.

To assess whether the accuracy of the parameter fitting

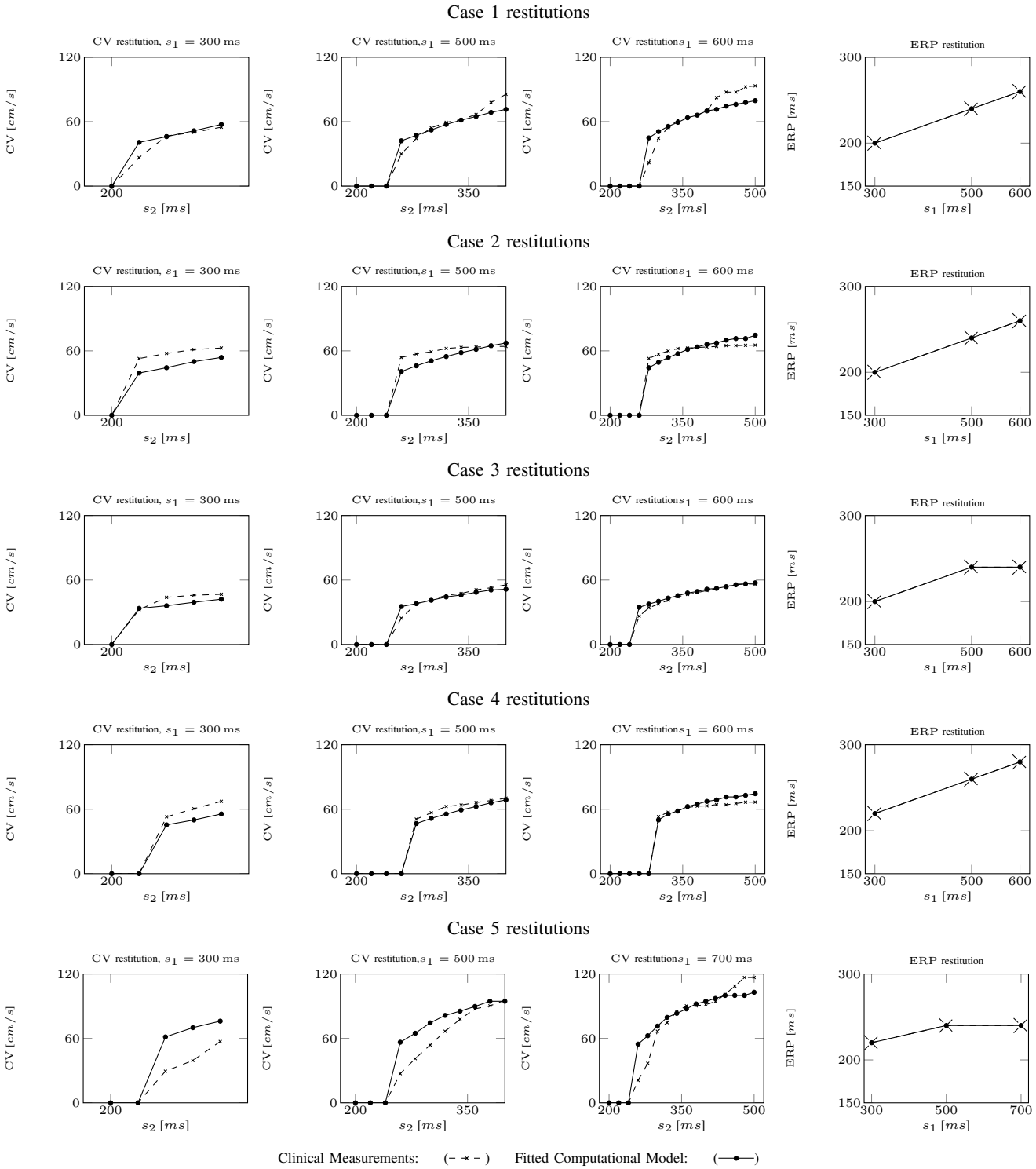


Figure 6. Case restitutions

would allow one to assess the regional differences in the electrophysiological properties of the atria, we compared the differences in the parameters fitted to clinical data within the context of the error estimated from the in silico study. The $95\%$ confidence interval for the error of the fitted diffusion coefficient, $\tau_{\text{in}}$, $\tau_{\text{out}}$, $\tau_{\text{open}}$ and $\tau_{\text{close}}$ from the in silico data is $40$, $45$, $100$, $45$ and $50\%$, respectively. In contrast, differences in parameter values in the clinical cases are up to $40$, $50$, $67$, $116$ and $35\%$ for diffusion coefficient, $\tau_{\text{in}}$, $\tau_{\text{out}}$, $\tau_{\text{open}}$ and $\tau_{\text{close}}$, respectively.

For the majority of parameters, the uncertainty in their estimated value is equal to or larger than the differences observed between clinical cases, reflecting the challenges in fitting parameters to sparse and noisy clinical data. The variation in the fitted $\tau_{\text{open}}$ values between clinical cases was larger than the uncertainty and could potentially be used to differentiate between tissue types.

### C. Application Example: Tissue characterization

Focal impulse and rotor mapping has recently been proposed as a novel ablation strategy [23], however this approach requires an expensive and large catheter and remains controversial. Encoding local tissue CV and ERP restitution properties within biophysical models provides a novel framework for predicting if local tissue properties are capable of supporting rotor or spiral activation patterns and may be useful in guiding ablation therapy. To predict if these tissue properties are compatible with supporting a re-entrant spiral activation pattern a spiral wave was initiated in a 2D simulation using a cross field stimulation pacing protocol with parameters from each of the 5 clinical cases. The original tissue properties were characterized by a point stimulus $s_1\_s_2$ pacing protocol. While the model parameters were screened to remove pacemaker activity, where a small region of tissue spontaneously self activates, the models can support re-entrant spiral wave activation patterns where a wave of activation forms a self sustaining reentrant circuit around the tissue (see movie 2). Models were simulated on 480 processors for 5000 ms taking 42 minutes of wall time. We observe three distinct spiral wave re-entrant activation patterns, as shown in Fig. 7: stable, meandering and breaking up. The only case to demonstrate spiral wave break up was Case 5, which had the largest discrepancy between modeled and measured CV restitution, particularly at high pacing frequencies (Fig. 6). The activation wave had a slower measured than modeled CV, which potentially allows a stable wave to exist in this tissue. Further cases would be required to confirm that we can reliably identify tissue that yields a predicted spiral wave break up. Rotor tip paths are shown for all cases in the supplement.

## IV. Discussion and perspectives

In this work we present a robust and clinically feasible protocol and fitting algorithm for characterizing local atria tissue electrophysiology properties using a MS ionic model.

Previous studies have aimed to fit MS parameters in the ventricles to patient data [18], [24]. Relan et al. [18], used analytic derivations of action potential duration (APD) restitution curves and CV measurement to fit 3 of the 5 MS model parameters. Corrado et al. [24], estimated $\tau_{\text{in}}$ and $\tau_{\text{out}}$ using a Kalman filter algorithm constrained by 12-lead ECG measurements. For parameters that were not fitted to patient data both studies used the default MS parameters, which were not derived from human data. In contrast, in this study all MS kinetic parameters were fitted to patient data. No error estimate was presented in these earlier studies so we cannot compare the relative accuracy of the different fitting approaches.

| Parameter | case 1 | case 2 | case 3 | case 4 | case 5 |
|---|---|---|---|---|---|
| diffusion coefficient $(\text{cm}^2/\text{s})$ | 1.0 | 1.0 | 1.0 | 1.4 | 1.4 |
| $\tau_{\text{in}}$ $(\text{ms})$ | 0.1 | 0.1 | 0.15 | 0.15 | 0.1 |
| $\tau_{\text{out}}$ $(\text{ms})$ | 2.5 | 1.5 | 2.5 | 2.5 | 2.5 |
| $\tau_{\text{open}}$ $(\text{ms})$ | 165 | 135 | 205 | 115 | 95 |
| $\tau_{\text{close}}$ $(\text{ms})$ | 115 | 155 | 115 | 145 | 115 |

Table II
ESTIMATED PARAMETERS FOR PATIENTS DATA SETS

For the fitting method presented here, error quantification using synthetic data found that and that the available measurements still resulted in fitting errors of $13.4 \pm 56.9\%$ for $\tau_{\text{out}}$, which is the least constrained parameter, while for $\tau_{\text{close}}$ and $\tau_{\text{open}}$ error were $(1.9 \pm 26.4\%)$ and $(2.2 \pm 22.1\%)$ respectively. All three of these parameters are constrained by repolarization, which was measured with a coarse resolution in order to minimize the time taken to make recordings. Decreasing the $s_2$ step size or the use of monophasic action potential catheters (MAP) [25], which provides a better measure of repolarization, may reduce the error in these parameters. However, reducing $s_2$ limits the clinical feasibility of the described protocol, while MAP catheters will not give CV measurements unless combined with a multi-electrode catheter,which poses an increase in procedural complexity.

Despite the uncertainty in some of the parameters, we were able to demonstrate that the fitted parameters captured the functionality of the desired parameter set (see Fig. 5). This allows us to use this parameter personalization approach to generate local ionic models for patient specific simulations of atrial function.

The uncertainty in fitted model parameters limits the ability to use the proposed approach to differentiate between tissue types. The data-base fitting protocol was designed to be efficient and robust for clinical applications. Increasing the resolution of the database, holding uncertain parameters fixed or using the data base fit as an initialization for a nonlinear optimization algorithm, such as Levenberg Marquardt, may improve the ability to differentiate between regional tissue types. However, the primary limitation is the weak sensitivity of the repolarization model parameters to the available clinical data. This is seen in Fig. 5, where the functionality is still captured, even in the presence of parameter uncertainties.

The measured maximum CV ranged between 60 and 100 cm\s (Fig. 6 ); these values are consistent with the values reported from clinical measurements [26]. Similarly, CV and ERP measurements are comparable with simulated restitutions generated from the more complex Courtermanche model [27].

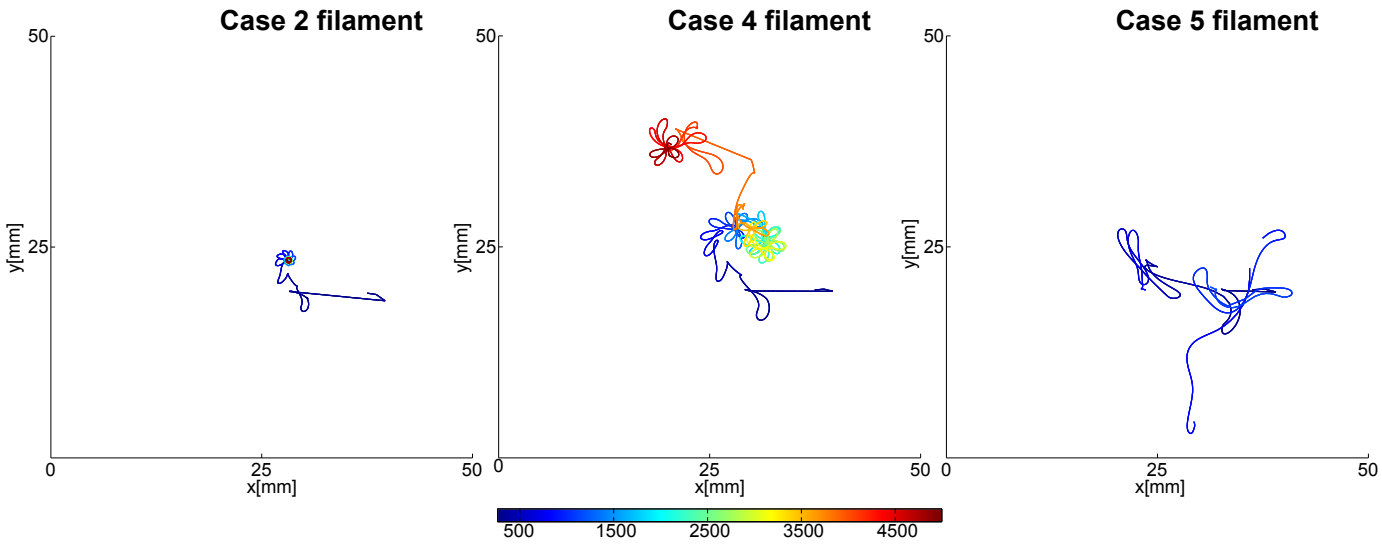


Figure 7. Path of the first filament for case 2,4 and 5. For cases 4 and 5 filaments are plotted until break-up occurred. Case 4 rotor breaks up after $t \simeq 3910\,\mathrm{ms}$ respectively. Case 5 shows an unstable spiral wave that breaks up rapidly into multiple wavelets before terminating at $t \simeq 1200\,\mathrm{ms}$. Color represents the time and is expressed in ms.

The variation in CV measured at different atrial locations [26], highlights the importance of personalized atrial models that reflect the heterogeneity in electrophysiological behavior seen throughout the atria.

The $\tau_{\mathrm{in}}$, $\tau_{\mathrm{out}}$ and diffusion coefficient values were the most consistent across cases. Notably $\tau_{\mathrm{in}}$ and $\tau_{\mathrm{out}}$ were lower in all cases than in the original ventricular MS model ($\tau_{\mathrm{in}} = 0.3$, $\tau_{\mathrm{out}} = 6.0$), where as the remaining fitted parameters spanned the original parameter values.

## V. Limitations

Clinical measurements are inherently noisy. By stimulating from the middle of the decapolar catheter we were able to record two potential data sets at each catheter location. However, due to noise and poor contact only the distal or proximal data sets were complete for any one location. The use of PentaRay catheters which provide five splines and 20 electrodes would result in higher density recordings and may improve the ability to characterize local electrophysiology properties.

Our model did not account for atrial curvature or wavefront curvature, both of which are likely to affect wave propagation. In the supplement we estimated the absence of wave curvature introduces an error of $6 - 10\%$ on CV calculation. To incorporate these factors into a model would require two, or even three, dimensional models or bespoke models for each case, which would require a new database of model simulations for each measurement. This would significantly increase the computational burden of our approach. We could refine the data set discretization to reduce the error of the parameter fitting. However, given the accuracy of the measurements available the current data base discretization provides a reasonable balance between accuracy and over fitting and allows us to formally state the accuracy of the model parameter predictions.

Due to the limited number of patient cases it is not possible to conclude that the distinct tissue types identified in this study are relevant to the general AF population. Further studies involving larger numbers of cases would be required to confirm this result.

The model does not provide a complete description of known atrial myocyte physiology and does not account for cardiac memory, [28], calcium dynamics [29] or the effects of the parasympathetic nervous system [30]. The modeling philosophy adopted here is to choose the simplest model with the smallest number of parameters that can fit the available data. The MS model was able to replicate all of the clinical data collected providing no motivation to use a more complex and less well constrained model.

The MS model exhibits pacemaker behavior in 0,1 and 2D simulations that was not present in any of the clinical data sets recorded. The presence of pacemaker behavior in the data base required the removal of a number of parameter sets. The stability of parameter sets was dependent on the dimensionality of the problem with some sets being stable in $0D$ and $1D$ simulations but unstable in $2D$. This property has been reported previously [19] and is not unique to the MS model. Parameter sweeps of mouse, [31] and rabbit [32] biophysical ionic models also identify unviable parameter sets that fail to repolarize or that show a pacemaker behavior. The introduction of a stability test addresses this issue. Pre calculating all $2D$ simulations is possible but comes at a high computational and data storage cost, so was not considered for this project but would reduce the parameter fitting process down to 1 minute.

## VI. Future Work

The proposed framework provides a pacing protocol and a method for rapidly and robustly creating models of local atrial tissue electrophysiology from clinical measurements. This approach has three potential clinical applications. Firstly, mapping the capacity of local tissue to support spiral waves

using a readily available decapolar catheter may offer a novel alternative to identifying spiral waves. Secondly, combining our approach with measures of atria tissue fibrosis [33], wall thickness [34] or epicardial fat [35] may allow non-invasive indicators of pathological tissue types to be identified. Finally, developing maps of cellular properties across the atria allows for the creation of personalized models that capture both the patient atria anatomy but also an individual's heterogeneous tissue properties for guiding diagnosis, optimizing therapies and predicting outcomes.

The aim of this study is to develop, characterize and demonstrate a novel protocol for creating electrophysiological model of local tissue properties. The application of this technique to a selected cohort of patients will enable us to draw general physiological conclusions on atria electrophysiology.

## VII. Conclusion

In this work we presented a robust and clinically tractable protocol and fitting algorithm for characterizing local atrial electro-physiology properties by biophysical ionic cell models. We validated the novel method by means of synthetic data and demonstrated its clinical potential by applying it to 5 data sets recorded from paroxysmal AF patients undergoing pulmonary vein isolation.

## Acknowledgment

This work made use of the facilities of ARCHER, the UK's national high-performance computing service, at the University of Edinburgh, and funded by the Office of Science and Technology through EPSRC's High End Computing Programme.

## References

[1] S. Colilla *et al.*, "Estimates of current and future incidence and prevalence of atrial fibrillation in the us adult population," *Am. J. Cardiol*, vol. 112, no. 8, pp. 1142–1147, 2013.

[2] M. Haïssaguerre *et al.*, "Electrophysiological breakthroughs from the left atrium to the pulmonary veins," *Circ.*, vol. 102, no. 20, pp. 2463–2465, 2000.

[3] C. Pappone *et al.*, "Atrial electroanatomic remodeling after circumferential radiofrequency pulmonary vein ablation: Efficacy of an anatomic approach in a large cohort of patients with atrial fibrillation," *Circ.*, vol. 104, no. 21, pp. 2539–2544, 2001.

[4] H. Oral *et al.*, "Pulmonary vein isolation for paroxysmal and persistent atrial fibrillation," *Circ.*, vol. 105, no. 9, pp. 1077–1081, 2002.

[5] R. Cappato *et al.*, "Worldwide survey on the methods, efficacy, and safety of catheter ablation for human atrial fibrillation," *Circ.*, vol. 111, no. 9, pp. 1100–1105, 2005.

[6] K. Nademanee *et al.*, "A new approach for catheter ablation of atrial fibrillation: mapping of the electrophysiologic substrate," *J. Am. Coll. Cardiol.*, vol. 43, no. 11, pp. 2044 – 2053, 2004.

[7] V. Swarup *et al.*, "Stability of rotors and focal sources for human atrial fibrillation: Focal impulse and rotor mapping (firm) of af sources and fibrillatory conduction," *J. Cardiovasc. Electrophysiol.*, vol. 25, no. 12, pp. 1284–1292, 2014.

[8] J. M. Miller *et al.*, "Initial independent outcomes from focal impulse and rotor modulation ablation for atrial fibrillation: Multicenter firm registry," *J. Cardiovasc. Electrophysiol.*, vol. 25, no. 9, pp. 921–929, 2014.

[9] M. O'Neill *et al.*, "The stepwise ablation approach for chronic atrial fibrillation-evidence for a cumulative effect," *J. Interv. Card. Electr.*, vol. 16, no. 3, pp. 153–167, 2006.

[10] P. Colli Franzone, L. Pavarino, and G. Savaré, "Computational electrocardiology: mathematical and numerical modeling," in *Complex Systems in Biomedicine*, A. Quarteroni, L. Formaggia, and A. Veneziani, Eds. Springer Milan, 2006, pp. 187–241.

[11] M. Potse *et al.*, "A comparison of monodomain and bidomain reaction-diffusion models for action potential propagation in the human heart," *IEEE Trans. Biomed. Eng.*, vol. 53, no. 12, pp. 2425–2435, 2006.

[12] L. Tung, "A bi-domain model for describing ischemic myocardial D–C potentials," Ph.D. dissertation, MIT, 1978.

[13] M. Ethier and Y. Bourgault, "Semi-implicit time-discretization schemes for the bidomain model," *SIAM J. Numer. Anal.*, vol. 46, no. 5, pp. 2443–2468, 2008.

[14] R. R. Aliev and A. V. Panfilov, "A simple two-variable model of cardiac excitation," *Chaos, Solitons & Fractals*, vol. 7, no. 3, pp. 293–301, 1996.

[15] C. Mitchell and D. Schaeffer, "A two-current model for the dynamics of cardiac membrane," *Bull. Math. Bio.*, vol. 65, pp. 767–793, 2003.

[16] J. F. Kaiser, "On a simple algorithm to calculate the 'energy' of a signal," in *Acoustics, Speech, and Signal Processing, 1988. ICASSP-88., 1988 International Conference on*, 1990, pp. 381–384.

[17] S. K. Mitra and Y. Kuo, *Digital signal processing: a computer-based approach*. McGraw-Hill New York, 2006, vol. 2.

[18] J. Relan *et al.*, "Coupled personalization of cardiac electrophysiology models for prediction of ischaemic ventricular tachycardia," *Int. Focus*, vol. 1, no. 3, pp. 396–407, 2011.

[19] M. Rioux and Y. Bourgault, "A predictive method allowing the use of a single ionic model in numerical cardiac electrophysiology," *ESAIM: Math. Model. Num. Anal.*, vol. 47, pp. 987–1016, 7 2013.

[20] R. N. Gutenkunst *et al.*, "Universally sloppy parameter sensitivities in systems biology models," *PLoS comp. bio.*, vol. 3, no. 10, p. e189, 2007.

[21] J. J. Waterfall *et al.*, "Sloppy-model universality class and the vandermonde matrix," *Phys. rev. lett.*, vol. 97, no. 15, p. 150601, 2006.

[22] K. S. Brown and J. P. Sethna, "Statistical mechanical approaches to models with many poorly known parameters," *Phys. Rev. E*, vol. 68, no. 2, p. 021904, 2003.

[23] S. M. Narayan *et al.*, "Focal impulse and rotor modulation ablation of sustaining rotors abruptly terminates persistent atrial fibrillation to sinus rhythm with elimination on follow-up: A video case study," *Heart Rhythm*, vol. 9, no. 9, pp. 1436 – 1439, 2012.

[24] C. Corrado, J.-F. Gerbeau, and P. Moireau, "Identification of weakly coupled multiphysics problems. application to the inverse problem of electrocardiography," *J. Comp. Phys.*, vol. 283, pp. 271 – 298, 2015.

[25] M. R. Franz, "Method and theory of monophasic action potential recording," *Prog. Cardiovasc. Dis.*, vol. 33, no. 6, pp. 347 – 368, 1991.

[26] F. M. Weber *et al.*, "Conduction velocity restitution of the human atrium-an efficient measurement protocol for clinical electrophysiological studies," *IEEE Trans. Biomed. Eng.*, vol. 58, no. 9, pp. 2648–2655, 2011.

[27] M. Courtemanche, R. J. Ramirez, and S. Nattel, "Ionic mechanisms underlying human atrial action potential properties: insights from a mathematical model," *Am. J. Physiol. Heart Circ. Physiol.*, vol. 275, no. 1, pp. H301–H321, 1998.

[28] D. G. Schaeffer *et al.*, "An ionically based mapping model with memory for cardiac restitution," *Bull. Math. Bio.*, vol. 69, no. 2, p. 459, 2007.

[29] C.-C. Chou *et al.*, "Intracellular calcium dynamics and anisotropic reentry in isolated canine pulmonary veins and left atrium," *Circ.*, vol. 111, no. 22, pp. 2889–2897, 2005.

[30] J. S. Floras, "Sympathetic nervous system activation in human heart failure: Clinical implications of an updated model," *J. Am. Coll. Cardiol.*, vol. 54, no. 5, pp. 375 – 385, 2009.

[31] J. O. Vik *et al.*, "Genotype-phenotype map characteristics of an in silico heart cell," *Front. Physiol.*, vol. 2, no. 106, 2011.

[32] O. J. Britton *et al.*, "Experimentally calibrated population of models predicts and explains intersubject variability in cardiac cellular electrophysiology," *Proc. Natl. Acad. Sci.*, vol. 110, no. 23, pp. E2098–E2105, 2013.

[33] N. F. Marrouche *et al.*, "Association of atrial tissue fibrosis identified by delayed enhancement mri and atrial fibrillation catheter ablation: The decaaf study," *JAMA*, vol. 311, no. 5, pp. 498–506, 2014.

[34] M. Bishop *et al.*, "Three-dimensional atrial wall thickness maps to inform catheter ablation procedures for atrial fibrillation," *Europace*, p. euv073, 2015.

[35] S. Sarin *et al.*, "Clinical significance of epicardial fat measured using cardiac multislice computed tomography," *Am. J. Cardiol*, vol. 102, no. 6, pp. 767–771, 2008.